MAGNETOHYDRODYNAMIC AND THERMAL ISSUES OF THE SiC_f/SiC FLOW CHANNEL INSERT

S. SMOLENTSEV,* N. B. MORLEY, and M. ABDOU
University of California, Department of Mechanical and Aerospace Engineering, 43-133 Engineering IV
Los Angeles, California 90095-1597

Received October 5, 2005
Accepted for Publication February 2, 2006

In the dual-coolant lead lithium (DCLL) blanket, the key element is the flow channel insert (FCI) made of a silicon carbide composite (SiC_f/SiC), which serves as electric and thermal insulator. The most important magnetohydrodynamic (MHD) and thermal issues of the FCI, associated with MHD flows and heat transfer in the poloidal channel of the blanket, were studied with numerical simulations using the U.S. DEMO DCLL design as a prototype. The mathematical model includes the two-dimensional momentum and induction equations for a fully developed flow and the three-dimensional (3-D) energy equation. Two FCI modifications, one with no pressure equalization openings and one with a pressure equalization slot, have been considered. The computations were performed in a parametric form, using the electric and thermal conductivity of the SiC_f/SiC as parameters. Under the DEMO reactor conditions, parameters of the FCI have been identified that result in low MHD pressure drop and low heat leakage from the breeder into the helium flows. This paper also discusses the role of the pressure equalization openings, 3-D flow effects, and the effect of SiC_f/SiC anisotropy.

KEYWORDS: *liquid metal blanket, magnetohydrodynamics, heat transfer*

I. INTRODUCTION

Flow channel inserts (FCIs) made of a silicon carbide composite (SiC_f/SiC) were first proposed by Tillack and Malang[1] as a means for electrical insulation between the flowing liquid metal and the load-carrying channel walls to reduce the magnetohydrodynamic (MHD) pressure drop in the long poloidal blanket channels of a fusion power reactor. High MHD pressure drop is a crucial point in almost all self-cooled and dual-coolant blanket concepts using liquid metal (Li or Pb-17Li) as a working fluid. The substantial increase in the pressure drop in conducting channels is caused by the interaction of the plasma-confining magnetic field with the electric current, induced in the flow domain that closes through the channel walls. The main attraction of the FCIs is that SiC_f/SiC has relatively low electrical conductivity, allowing for sufficient reduction of the induced electric currents by decoupling the liquid metal flow from the walls. Another potential advantage of the FCI is related to low thermal conductivity of the SiC_f/SiC, which allows for the reduction of heat losses from the breeder and therefore high bulk temperatures at the blanket exit, making the overall thermal efficiency of the blanket higher. At the same time, the FCI does not serve as a structural element and carries only low primary static (its own weight floating in the liquid metal) and secondary (thermal) stresses, which are expected to be within allowable limits. At present, the idea of using the FCI as both electric and thermal insulator takes central place in several European and U.S. blanket concepts, with Pb-17Li as a breeder and ferritic steel as a structural material.[2–4] This concept is also a candidate for blanket tests in ITER (Ref. 5).

In the paper, we address MHD and thermal issues associated with liquid metal flows in a blanket channel with the SiC_f/SiC FCI under conditions of the U.S. DEMO dual-coolant lead lithium (DCLL) blanket.[4] The fusion power of the DCLL is 2116 MW. The peak outboard neutron wall loading is 3.72 MW/m^2, and the peak surface heat flux at the outboard midplane is 0.5 MW/m^2. In this design, reduced activation ferritic steel is used as the structural material. Helium is used to cool the first wall and the blanket structure, and the self-cooled breeder, Pb-17Li, circulates for power conversion and tritium breeding. A key element of the concept is the SiC_f/SiC FCI, which serves as electric insulator to reduce the impact from the MHD pressure drop of the circulating liquid metal, and as thermal insulator to separate the

*E-mail: sergey@fusion.ucla.edu

high-temperature Pb-17Li from the helium-cooled ferritic structure.

A sketch of a typical blanket channel with the FCI is shown in Fig. 1. The FCI is seated inside the blanket channel, forming a thin gap with the channel walls. Both the gap and the space inside the FCI are filled with flowing Pb-17Li driven by the same pressure head. In what follows, we will refer to the flow inside the FCI as "bulk flow" and that in the space between the FCI and the ferritic wall as "gap flow." We will also distinguish different sections of the gap. The gaps oriented with the long side perpendicular to the applied magnetic field are called here "Hartmann gaps." The other two gaps, parallel to the magnetic field, are called "side gaps." These terms have been adopted from the analogous terms "Hartmann walls" and "side walls" commonly applied to MHD flows in rectangular channels. The channels sizes are identified here with the internal dimensions of the FCI.

The basic dimensions and other related parameters of the reference blanket are given in Ref. 4 and are also summarized here in Table I. The most important dimensionless parameters are the Reynolds number, $\mathrm{Re} = U_0 b/\nu$, and the Hartmann number, $\mathrm{Ha} = B_z^0 b(\sigma/\nu\rho)^{0.5}$, defined through the mean bulk velocity U_0, toroidal magnetic field B_z^0, half of the channel width b, and physical properties of the liquid: density ρ, electrical conductivity σ, and kinematic viscosity ν. In the reference blanket flow, $\mathrm{Ha} = 15\,900$ and $\mathrm{Re} = 83\,700$.

One of the main goals of the study is to assess insulating properties of the FCI and to analyze its effect on the velocity and temperature distribution in the blanket channel by doing parametric calculations with the electric and thermal conductivity of $\mathrm{SiC}_f/\mathrm{SiC}$ as parameters. Earlier, MHD analysis for a flow with the $\mathrm{SiC}_f/\mathrm{SiC}$ FCI was performed for the European conceptual dual-coolant blanket.[6] Some calculation results for the DEMO blanket are also presented in Ref. 7, but in a limited form. In Ref. 6, the gap, the ferritic wall, and the openings in the FCI are not considered. The effect of the FCI on the bulk flow was simulated via a special boundary condition derived in Ref. 8. One of the interesting observations in Ref. 6 is reduction of the high-velocity jets near the side walls as the electric conductivity of the insert decreases. Unlike Ref. 6, the present MHD analysis is applied to the whole cross-sectional area of the blanket channel, which includes not only the bulk flow but also the FCI, the ferritic wall, and the gap. Adding these details is important because the effect of the gap flow on heat transfer and consequent heat losses can be noticeable.

TABLE I

Parameters for the Flow in the Front Poloidal Channel of the Reference DCLL Blanket

Poloidal length	2 m
Channel sizes	$2b = 0.3$ m (toroidal), $2a = 0.2$ m (radial)
FCI thickness	0.005 m
Gap width	0.002 m
Ferritic wall thickness	0.005 m
PES width	0.005 m
Toroidal magnetic field (outboard)	4 T
Pb-17Li mean flow velocity	0.06 m/s
Helium temperature	400°C
Inlet/outlet Pb-17Li temperature	460/660°C
Heat transfer coefficient in helium	4000 $\mathrm{W/m^2 \cdot K}$

II. TWO MECHANISMS OF PRESSURE EQUALIZATION

Pressure equalization is an important component of the FCI concept. In the original concept,[1] a thin slot in one of the FCI walls, as shown in Fig. 1, was proposed to equalize the pressure on both sides of the FCI, thus reducing or even fully eliminating primary stresses in the insert. This is called the pressure equalization slot (PES). Another possible approach is to make small discrete pressure equalization holes (PEHs). The width and location of the PESs as well as the size, location, and spacing between the holes in the PEH case is a subject of optimization since increasing the area of the openings not only will provide better pressure equalization but also may lead to more significant current and heat leakage into the gap and ultimately into the ferritic structure.

In a strong reactor magnetic field, the hydrodynamic entry length is strongly reduced in comparison with non-MHD flows.[9] It appears that the flow development length decreases as the interaction parameter, $N = \mathrm{Ha}^2/\mathrm{Re}$, increases. In the reference flow, the interaction parameter is as high as 3020. This gives a ground to expect that at a distance of a few characteristic channel dimensions from the inlet, the flow becomes fully developed or at least close enough to the fully developed state, so that the fully developed flow model seems to be applicable. In fact, the fully developed flow model is in common use, when addressing poloidal flows in a blanket. However, correctness of this assumption still needs more validations, which will require three-dimensional (3-D) calculations or experimental studies.

The 3-D effects are discussed at a qualitative level in Sec. VIII. A qualitative sketch of the pressure distribution in a blanket channel in a steady regime is suggested in Fig. 2. In the fully developed flow, the pressure is uniform over the whole cross-sectional area. No pressure difference between the gap and the bulk appears. However, within the entry length, where the flow is developing, the pressure in the gap is not necessarily equal to that in the bulk flow. Nevertheless, as conceived by the authors of the original FCI concept, this pressure difference will not be intolerably high. The reduction is supposed to occur due to the pressure equalization effect associated with the flows of the liquid

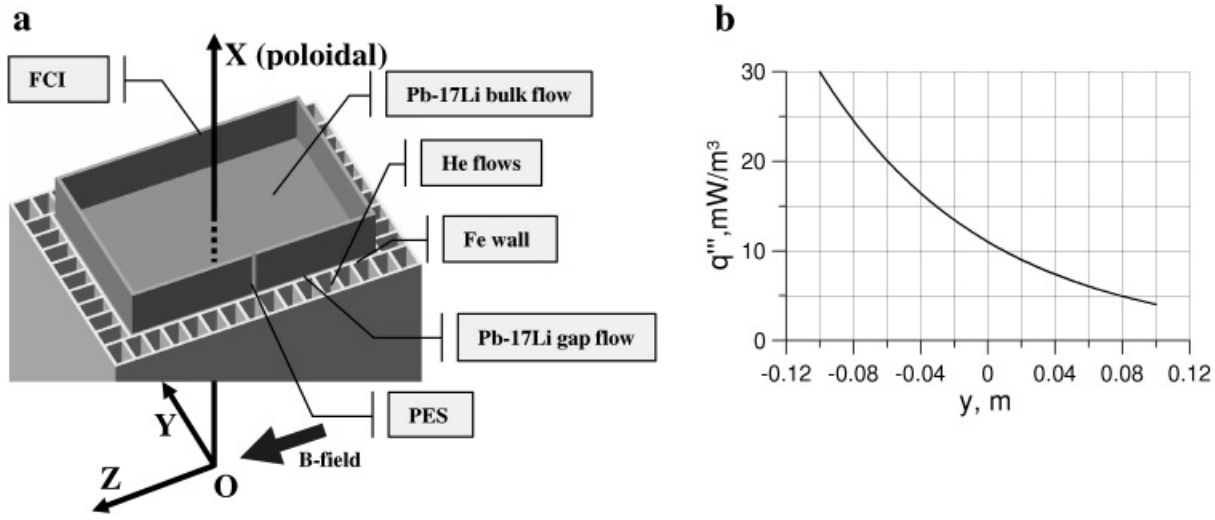

Fig. 1. Typical poloidal blanket channel with (a) FCI and helium cooling channels and (b) volumetric heating.

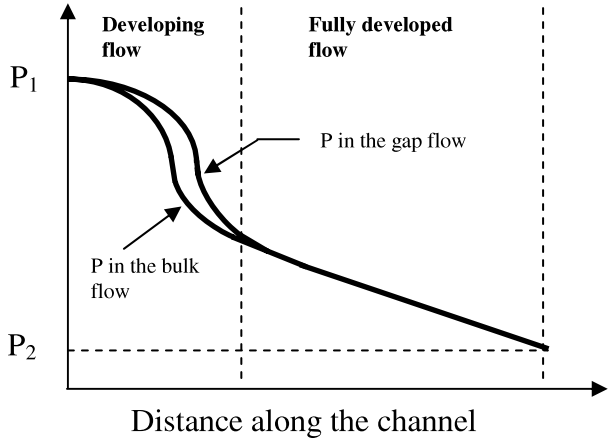

Fig. 2. Axial pressure variation in the bulk flow and in the gap.

through the pressure equalization openings, for example, from the gap to the bulk. Such an interpretation of the pressure equalization mechanism is, however, purely hydrodynamic and does not take into account electromagnetic effects, which seem to be very important in forming the pressure field.

The importance of the electromagnetic effects on the pressure equalization can be illustrated via the Poissson equation for pressure, which can be derived by taking a derivative of each projection of the momentum equation with respect to the corresponding coordinate and then adding all these equations together:

$$\frac{\partial^2 P}{\partial x^2} + \frac{\partial^2 P}{\partial y^2} + \frac{\partial^2 P}{\partial z^2} = S_p^V + S_p^J \ . \qquad (1)$$

Equation (1) is written in the Cartesian coordinates x, y, and z; S_p^V and S_p^J are source terms. The first source term is associated with the fluid motion:

$$S_p^V = \rho \frac{\partial}{\partial x}\left[\nu\nabla^2 U - U\frac{\partial U}{\partial x} - V\frac{\partial U}{\partial y} - S\frac{\partial U}{\partial z}\right] + \rho \frac{\partial}{\partial y}\left[\nu\nabla^2 V - U\frac{\partial V}{\partial x} - V\frac{\partial V}{\partial y} - W\frac{\partial V}{\partial z}\right] + \rho \frac{\partial}{\partial z}\left[\nu\nabla^2 W - U\frac{\partial W}{\partial x} - V\frac{\partial W}{\partial y} - W\frac{\partial W}{\partial z}\right] . \qquad (2a)$$

The second term is of electromagnetic nature and stands for the changes in the pressure due to electric current flows:

$$S_p^J = \frac{\partial}{\partial x}(j_z B_y^0 - j_y B_z^0) + \frac{\partial}{\partial y}(j_x B_z^0 - j_z B_x^0) + \frac{\partial}{\partial z}(j_y B_x^0 - j_x B_y^0) \ , \qquad (2b)$$

where $\mathbf{j}$ (j_x, j_y, j_z) denotes the induced electric current density vector and $\mathbf{B}_0$ (B_x^0, B_y^0, B_z^0) is the applied magnetic field. As related to S_p^J, a pressure equalization mechanism is possible through electric currents flowing from higher to lower potential regions. Once the pressure is changed locally, the electric potential will follow the pressure changes, driving the electric currents that tend to recover the pressure balance. Such electric current flows are special in two ways. First, the currents can flow not only through the openings but also through the FCI. Second, all changes in the current

flows occur almost immediately, while the liquid flows through the openings have a much larger timescale. The electromagnetic pressure equalization mechanism will therefore be especially important in transient events (i.e., plasma disruptions), while the hydrodynamic mechanism under disruptions conditions is almost ineffective due to relatively slow flow response.

III. MATHEMATICAL MODEL AND COMPUTER CODE

The present analysis is applied to long poloidal channels, where the MHD pressure drop is mostly related to cross-sectional currents. Insulation, such as FCIs, reduces the cross-sectional currents. In other elements of the blanket, such as manifolds, bends, etc., the flow is essentially 3-D; the MHD pressure drop is mostly caused by axial currents, which cannot be eliminated by the FCI. Such elements are thus not considered here.

A full mathematical model for the flows in the poloidal ducts of the blanket is generally 3-D. There are many reasons why the flows can be different from two-dimensional (2-D) (see discussion in Sec. VIII). Among the most important ones are the already mentioned inlet flow effects. However, over the major section of the channel, the flow is believed to be close to being fully developed. Also, the transient effects are not considered here. The present MHD model is therefore steady state and 2-D, while the temperature field is 3-D. The problem is then governed by 2-D momentum, 2-D induction, and 3-D energy equations, formulated in terms of the flow velocity (U), induced magnetic field (B_x), and temperature (T). The fully developed MHD flow equations have been used for decades (e.g., Ref. 10). The only difference of the equations used in the paper with the standard formulation is placing the electrical conductivity inside the derivative in the induction equation. This allows for treating a multimaterial domain without using internal boundary conditions at the interfaces. However, this additional feature does not add any complexity to the derivations. That is why the governing equations are shown here in the final form:

$$\nu\left(\frac{\partial^2 U}{\partial z^2}+\frac{\partial^2 U}{\partial y^2}\right)-\frac{1}{\rho}\frac{dP}{dx}+\frac{B_z^0}{\rho\mu_0}\frac{\partial B_x}{\partial z}=0\ , \qquad (3)$$

$$\frac{1}{\mu_0}\frac{\partial}{\partial z}\left(\frac{1}{\sigma_y}\frac{\partial B_x}{\partial z}\right)+\frac{1}{\mu_0}\frac{\partial}{\partial y}\left(\frac{1}{\sigma_z}\frac{\partial B_x}{\partial y}\right)+B_z^0\frac{\partial U}{\partial z}=0\ , \qquad (4)$$

and

$$\rho C_p U\frac{\partial T}{\partial x}=\frac{\partial}{\partial x}\left(k_x\frac{\partial T}{\partial x}\right)+\frac{\partial}{\partial y}\left(k_y\frac{\partial T}{\partial y}\right)+\frac{\partial}{\partial z}\left(k_z\frac{\partial T}{\partial z}\right)+q_T'''\ . \qquad (5)$$

The coordinates x, y, and z denote the poloidal, radial, and toroidal distances (Fig. 1). The x-axis coincides with the channel axis. The coordinate origin is located in the bottom plane, at the flow inlet. The other notations are standard. Equation (3) is formulated for the Pb-17Li only, while Eqs. (4) and (5) are written over the whole domain, including the FCI, ferritic wall, gap, and the bulk flow. The grid structure of the helium cooling channels is not reproduced in detail but is modeled as a wall of a uniform thickness. The source term q_T''' stands for volumetric heating. The electric and thermal conductivity, σ and k, are assumed to be coordinate dependent to introduce anisotropy in the material properties of the silicon carbide. The following notations are used for the electric conductivity of the silicon carbide composite along and across the fibers: $\sigma_\parallel$ and $\sigma_\perp$. With these notations, $\sigma_z=\sigma_\perp$ and $\sigma_y=\sigma_\parallel$ in the Hartmann walls, while $\sigma_z=\sigma_\parallel$ and $\sigma_y=\sigma_\perp$ in the side walls.

To solve Eqs. (3) and (4), a numerical code[11] was used. The code has been specially designed for channels with a "sandwich" structure of several materials with different material properties. The code includes a finite-volume formulation, automatically generated Hartmann number sensitive meshes, and an effective convergence acceleration technique. To capture the multimaterial structure of the domain, block-structured grids matching at the interfaces were used. Tests performed at Ha $\sim 10^4$ have shown very good accuracy.[11]

Three types of SiC_f/SiC FCIs with regard to the pressure equalization openings are analyzed in the paper: (a) FCI without any openings and those with the pressure equalization slot either in the (b) Hartmann or (c) side wall. In all PES cases, the slot is located in the center of the FCI wall and is 5 mm wide. The PEH case is not given special treatment since the holes (if far apart) are expected to have only local disturbances on the flow. Therefore, the PEH case is treated in the same way as the case with no openings. At present, effects due to anisotropy in k_{SiC} have not been analyzed, assuming $k_x=k_y=k_z=k_{SiC}$. All calculations were performed for the flow in the front blanket channel.

One MHD computation takes from a few hours to 3 days with a 2.4-MHz personal computer. The computational time is strongly dependent on the electric conductivity of SiC_f/SiC and on the location of the pressure equalization slot. Examples of the computational mesh are shown in Fig. 3. In the case with no openings, the computational mesh includes 215 × 215 points (101 × 101 points in the bulk flow, 27 across the gap, 15 across the wall, and 15 across the FCI). Extra grid points are added in the PES cases to have better resolution in the slot region, where both the induced magnetic field and velocity are very nonuniform. The mesh generation procedure used in the code places from about one-fourth to one-third of all grid points across the Hartmann layer, so that each Hartmann layer is resolved with about 15 points

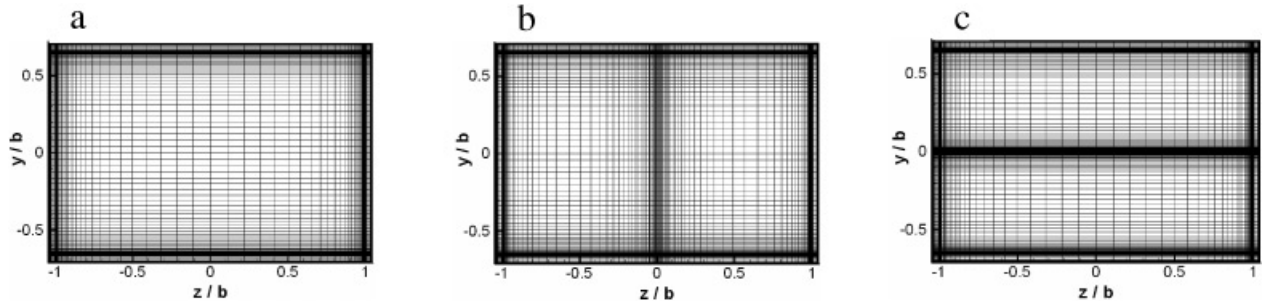

Fig. 3. Computational mesh in MHD calculations: (a) no openings, (b) PES in the side wall, and (c) PES in the Hartmann wall.

across. After completing the MHD calculation, the velocity profile is used as input data for solving Eq. (5). The source term in Eq. (5) is determined independently from neutronics calculations, where the detailed radial build is modeled using the DANTSYS neutron and gamma transport code.[12] The neutronics results for the radial variation of nuclear heating are then approximated in the following form (Fig. 1b):

$$q'''_T = q_0 \,\mathrm{Exp}\left(-m\,\frac{y+a}{a}\right) . \qquad (6)$$

The parameters q_0 and m are determined by comparisons with the calculated data.

IV. MATERIAL PROPERTIES OF SiC_f/SiC

Material properties of a composite depend significantly on the fabrication techniques, impurities, dopants, and interphase materials. For example, the electric conductivity for a sample fabricated by polymer impregnation pyrolysis is $\sigma_{SiC} = 22$ S/m, while samples made by chemical vapor infiltration demonstrate much higher conductivity: $\sigma_{SiC} = 650$ S/m as summarized in Ref. 13. The recommended value of the thermal conductivity in Ref. 13 is $k_{SiC} = 15$ W/m·K for typical 3-D low-porosity composites. Lower values can be achieved with a 2-D woven, lower-density composite. Some change in σ_{SiC} and k_{SiC} has been reported under neutron irradiation conditions.[14] Current data on the thermal conductivity for many 2-D and 3-D composites, including results of the irradiation tests, are presented in Ref. 15. Significant changes of the effective material properties are possible due to infiltration of liquid metal into pores. One should also take into account differences in material properties along and across the fibers. Current measurements of the electric conductivity of the conventional 2-D composite have shown that it is highly anisotropic.[16] For example, at 500 and 800°C, the electric conductivity along the fibers was 380 and 500 S/m, whereas across the fibers it was 1.0 and 7.5 S/m, respectively.

In the present study, we perform calculations in a parametric form using values presented above as the starting point. The electrical conductivity of the SiC_f/SiC varied from 0.01 to 500 S/m, and thermal conductivity varied from 2 to 20 W/m·K. Advice from material experts indicates that the lower values at ~1 S/m and 1 W/m·K are in fact achievable. A thin sealing layer of crystal SiC was assumed at all surfaces of the FCI to prevent penetration of liquid metal in the pores. Effects due to microdefects in the sealing layer and infiltration into pores are not presently considered.

V. MHD FLOW

Results of calculations for three types of the flow insert are presented in Secs. V.A and V.B. All results are computed at $\sigma_z = \sigma_y = \sigma_{SiC}$ since the effect of anisotropy was found to be small. Comments and some calculation results for anisotropic FCIs are given in Sec. V.D.

V.A. No Pressure Equalization Openings

The typical velocity profile and induced magnetic field distribution are shown in Fig. 4. The electric current induced in the core of the bulk region crosses the side FCI walls in the normal direction. After leaving the FCI, the electric current turns at almost 90° and flows tangentially through the gap and the wall. A characteristic feature of the flow is two high-velocity jets near the side walls, which carry most of the volumetric flow rate. Appearance of the near-wall jets is a typical manifestation of the MHD effects in electrically conducting ducts or ducts with imperfect insulation. Many examples of "M-type" ("U-type") velocity profiles and explanations for the mechanism of the jet formation can be found in the MHD literature (e.g., Ref. 10). Although Ref. 10 does not specifically address flows with FCI, the mechanism leading to the jet formation in the reference case is essentially the same. Special numerical and asymptotic analysis for ducts with thin insulating coatings, also showing the jet flows, is performed in Ref. 17. It is noticeable that the

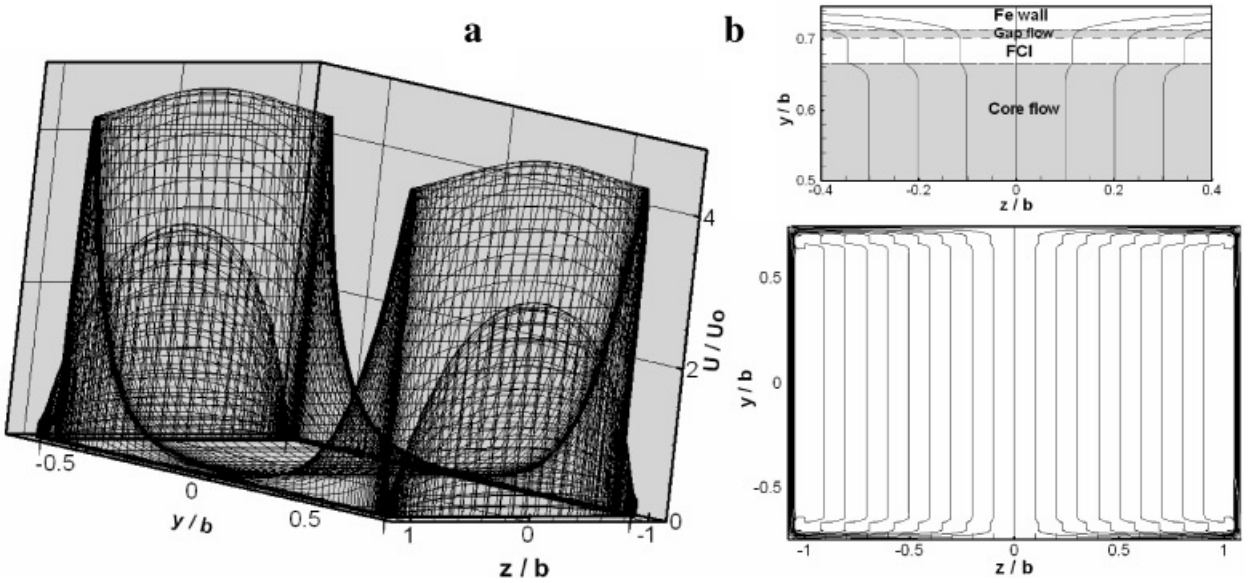

Fig. 4. (a) Velocity distribution in the bulk and gap and (b) induced magnetic field contour plot over the whole cross-sectional area of the blanket channel in the flow without openings in the FCI at σ_{SiC} = 100 S/m.

present analysis shows significant differences in the flow in the two different sections of the gap. In the side gap, where the electric current is mostly parallel to the magnetic field, the velocity is comparable with the near-wall jets, and the velocity profile is close to parabolic. In the Hartmann gap, the velocity is of a Hartmann type, and the flow is almost stagnant. As the electric conductivity of the silicon carbide composite decreases, the effect of electromagnetic coupling between the flow in the gap and the bulk flow reduces; the velocity in the gap drops relative to the mean velocity in the bulk region (Figs. 5a and 5b). One can also observe strong reduction of the near-wall jets as σ_{SiC} decreases (Fig. 5c). However, even at σ_{SiC} = 5 S/m, the jet flow still exists, showing that the FCI is not a perfect insulator.

V.B. PES in the Hartmann Wall

All major flow features observed in the case with no openings, such as near-wall jets, are essentially the same. The main differences are local and occur within a narrow area adjacent to the slot (Fig. 6). In this area, the induced

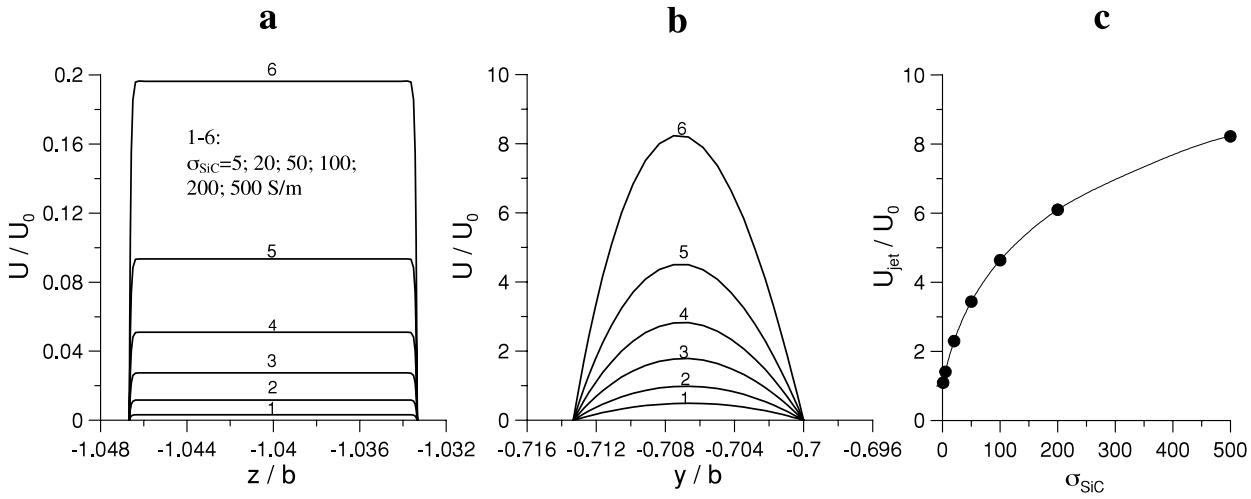

Fig. 5. Effect of σ_{SiC} on the flow in the Hartmann gap at (a) $y = 0$, (b) side gap at $z = 0$, and (c) the near-wall jet.

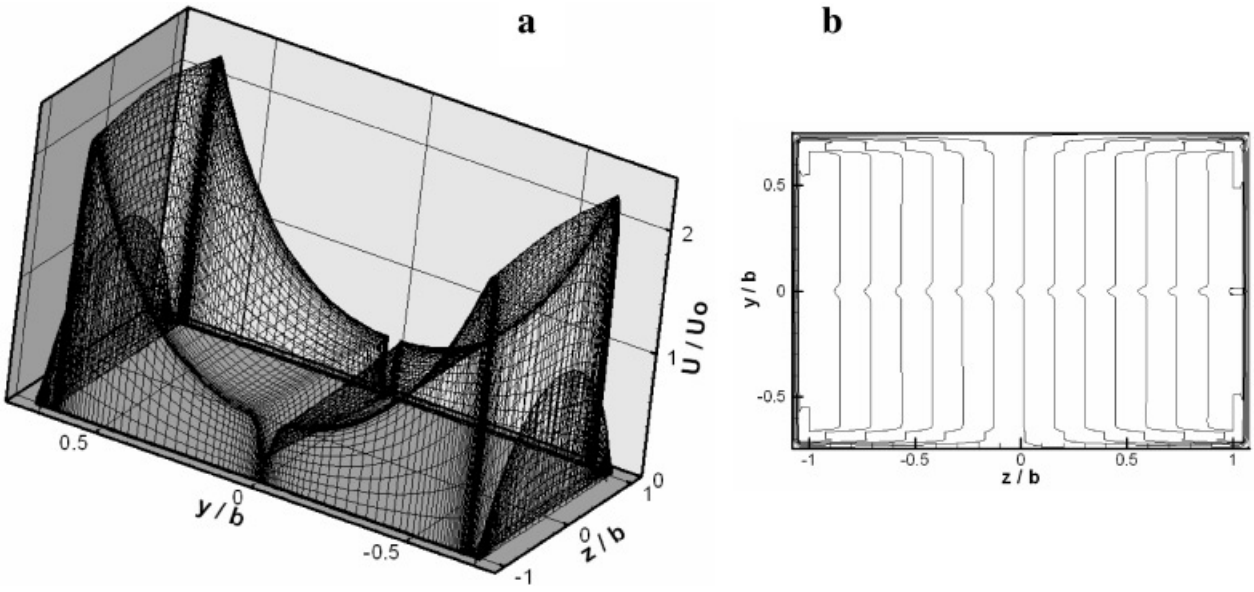

Fig. 6. (a) Velocity distribution in the bulk and gap and (b) induced magnetic field contour plot over the whole cross-sectional area of the blanket channel in the flow with PES in the Hartmann wall of the FCI at $\sigma_{SiC} = 20$ S/m. The PES is located at $z = -b$, $y = 0$.

magnetic field counter lines are slightly disturbed, and the velocity profile exhibits a velocity deficit zone, stretching from the wall with the slot at $z = -b$ to the opposite Hartmann wall.

V.C. PES in the Side Wall

Rather than flowing across the FCI, the electric currents flow mostly through the slot, which exhibits lower electric resistance than the FCI (Fig. 7). In the slot, the electric current flows perpendicular to the magnetic field lines, resulting in a strong flow-opposing Lorentz force, which turns the flow in the opposite direction. An enlarged view of the velocity profile (Fig. 8) shows that in the near-slot area, the flow has a rather complex structure. The reverse flow jet appears both in the gap and in the bulk region in the immediate vicinity of the slot. The slot also affects the near-wall jet, which is sufficiently reduced as compared to the other jet at the opposite wall, which seems not to be affected by the slot. However, in practice, the reverse flow will most likely be modified through a convective motion. The flow will likely be unstable due to the inflection points in the main velocity profile. As the electric conductivity of the FCI decreases, the reverse flow in the near-slot area also decreases.

V.D. MHD Pressure Drop

Calculations of the MHD pressure drop are presented in Fig. 9a in the form of the pressure drop reduction factor R as a function of σ_{SiC} for all three FCI types. The pressure drop reduction factor is defined as

$$R = \frac{(dP/dx)_0}{dP/dx} \ ,$$

where $(dP/dx)_0$ is the pressure gradient in the same flow without the FCI. All FCI types show high electric insulation. Perfect insulation under the reference conditions is achieved at $\sigma_{SiC} \sim 0.01$ S/m, giving a maximum pressure drop reduction factor of about 700 regardless of the FCI type. However, it is unlikely that the real SiC composites can demonstrate electric conductivity lower than 1 S/m, even under the neutron irradiation effect. Higher-conductivity composites with realistic values of σ_{SiC} from 1 to 20 S/m can result in a pressure reduction factor from 50 to ~400, which is also quite affordable. The reduction factor in the case with the PES in the Hartmann wall demonstrates no differences with the case without openings, while the reduction factor in the case with the PES in the side wall is lower. The differences in the reduction factor among the three FCI types can be seen for σ_{SiC} from 0.1 to 20 S/m. The maximum difference, by a factor of 2, is observed at $\sigma_{SiC} = 1$ S/m. Providing that the real values of the electric conductivity are in the range of 1 to 20 S/m, the case with the slot in the Hartmann wall looks more attractive as compared to the case with the slot in the side wall. One more reason in favor of this case is the velocity profile without a reverse flow, as seen in Fig. 6. Additional calculations of the MHD pressure drop were performed assuming no flow in the gap. These

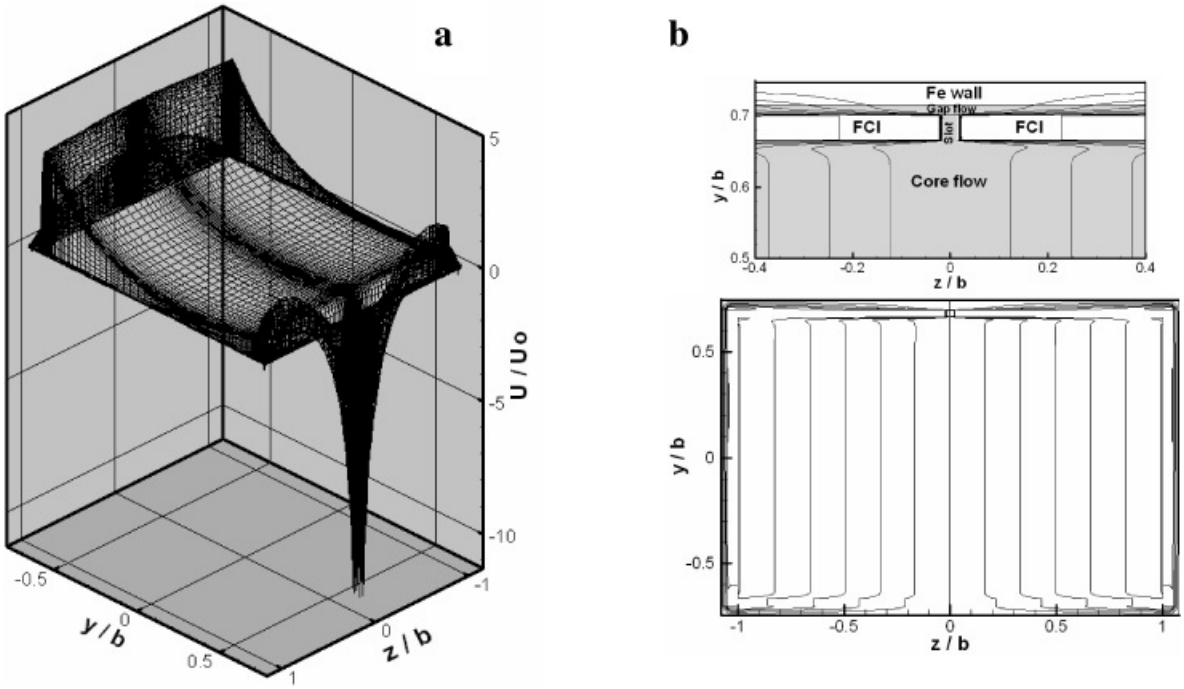

Fig. 7. Velocity distribution in (a) the bulk and gap and (b) induced magnetic field contour plot over the whole cross-sectional area of the blanket channel in the flow with PES in the side wall of the FCI at $\sigma_{SiC} = 20$ S/m.

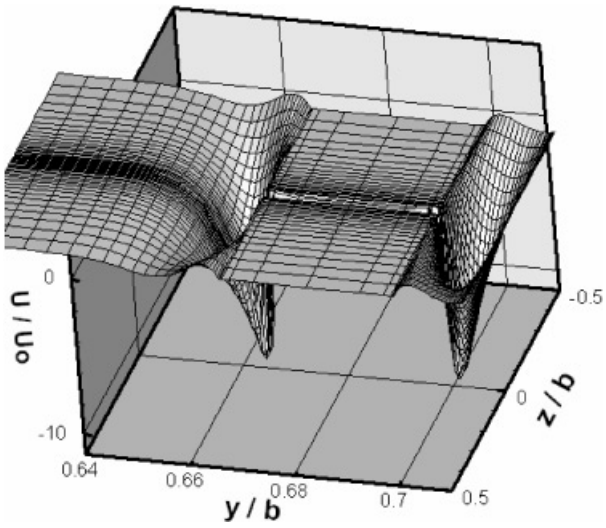

Fig. 8. Detailed view of the velocity profile shown in Fig. 7 in the immediate vicinity of the slot.

calculations showed that the flow in the gap has almost no effect on the pressure drop.

The effect of anisotropy in electric conductivity on the pressure drop is shown in Fig. 9b, where the pressure gradient in the flow without FCI is scaled with $(dP/dx)^*$, which is calculated at $\sigma_{\parallel} = \sigma_{\perp}$. As the ratio $\sigma_{\parallel}/\sigma_{\perp}$ increases, the MHD pressure drop slightly increases since more electric currents flow in the FCI. The pressure drop increase, however, is small even at $\sigma_{\parallel}/\sigma_{\perp} \sim 10^2$. In real 2-D composites, it is likely that $\sigma_{\parallel}/\sigma_{\perp}$ will not be higher than $\sim 10^1$ to 10^2. Therefore, as a first approximation, the effect of anisotropy on the blanket flow can be neglected.

VI. HEAT TRANSFER

The main goal of the analysis was to study the effect of σ_{SiC} and k_{SiC} on heat transfer in the domain that includes the bulk and gap flows, FCI, and the ferritic wall. The key points in the heat transfer optimizations are (a) minimization of heat losses from the liquid metal into the helium flows; (b) reduction of temperature stresses associated with the temperature gradient across the FCI; and (c) reduction of the temperature at the interface between the ferritic wall and Pb-17Li in the gap below its corrosion limit, which is ~500°C.

Three-dimensional heat transfer simulations were performed for the case with no openings in the FCI. In the present analysis, the temperature in the helium flows was fixed at 400°C, and the heat transfer coefficient in the helium flow was estimated at 4000 W/m^2·K, using a standard correlation for the Nusselt number under conditions of a turbulent helium flow in the reference blanket. The typical temperature distribution in the channel is

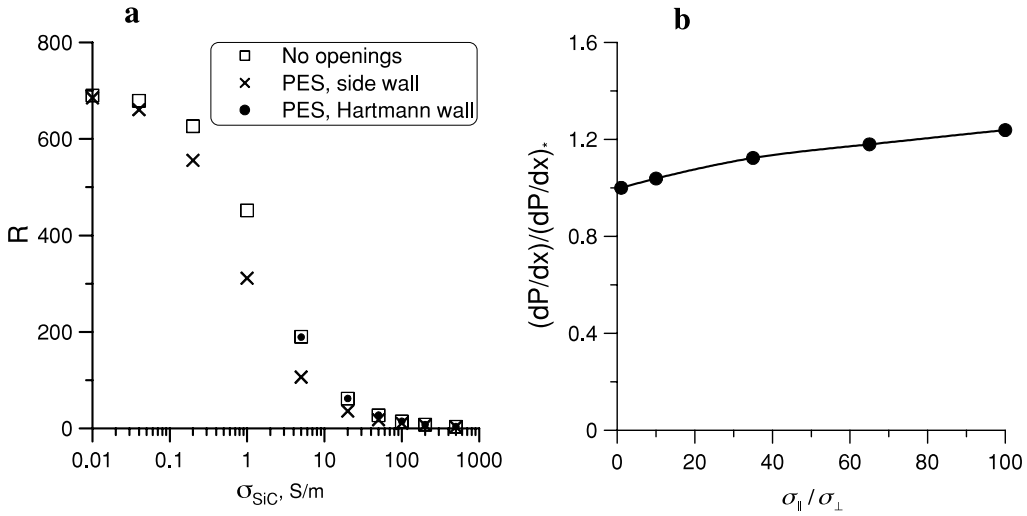

Fig. 9. MHD pressure drop in the flow with FCI. (a) Effect of the electrical conductivity of the SiC composite on the pressure drop reduction factor. (b) Effect of anisotropy in the electrical conductivity on the MHD pressure drop at $\sigma_{\perp} = 20$ S/m.

shown in Fig. 10. Intense temperature variations occur in the radial direction. Changes in the temperature field in the toroidal direction are small in the central region but very large at the edges of the domain, where the ferritic structure is cooled by the helium flows. The temperature also changes in the poloidal direction due to the transport of heat by the liquid metal flow. Maximum temperatures are achieved at the flow exit. Temperatures at the edges of the domain are mostly controlled by the helium flows, while in the central part of the domain by the liquid metal flow.

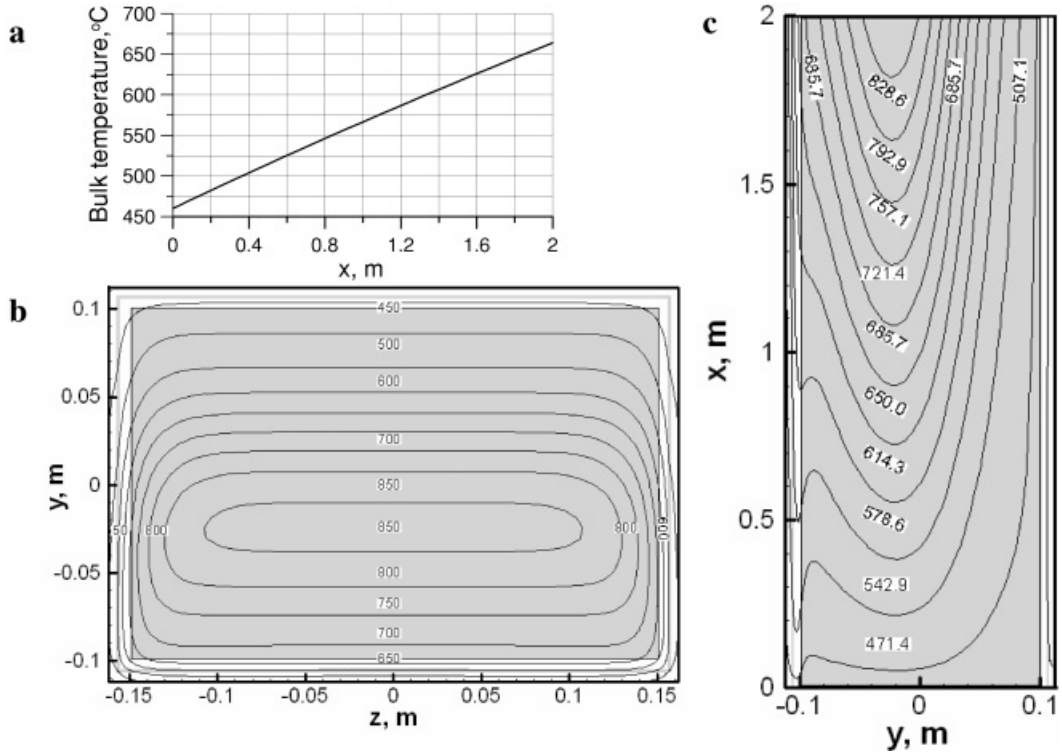

Fig. 10. Temperature field in the blanket channel at $\sigma_{SiC} = 20$ S/m, $k_{SiC} = 15$ W/m·K: (a) bulk temperature, (b) cross-sectional temperature distribution at the exit, and (c) temperature distribution in the poloidal-radial plane.

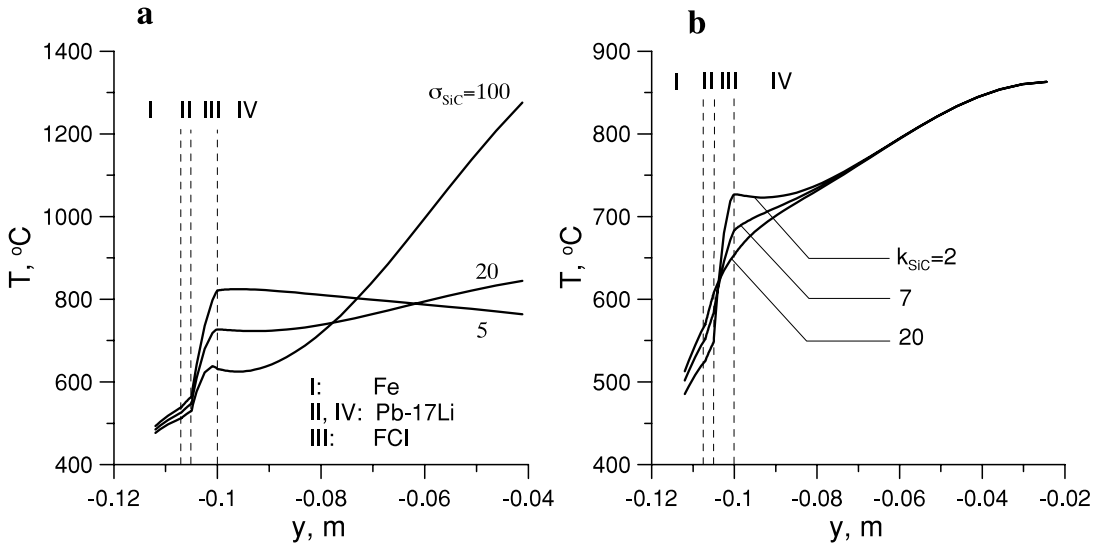

Fig. 11. Radial temperature distribution in the vicinity of the front wall at the flow exit at (a) k_{SiC} = 2 W/m·K and (b) σ_{SiC} = 20 S/m.

Figure 11 shows the effect of σ_{SiC} and k_{SiC} on the radial temperature distribution at the channel exit in a region facing the first wall, where the most heat deposition occurs. The region includes the ferritic wall, side gap, FCI, and a part of the bulk flow. Both k_{SiC} and σ_{SiC} have a strong effect on the temperature field. The effect of k_{SiC} is obviously thermal insulation of the bulk flow from the helium flows. The influence of σ_{SiC} is not so simply explained since its variations result in significant changes of heat transfer conditions through modifications of the liquid metal flows on both sides of the FCI. The heat flux at the interface between the FCI and Pb-17Li in the bulk flow can correspondingly be either inward or outward. It is also noticeable that the effect of k_{SiC} on the temperature field is local, while σ_{SiC} affects the temperature over the whole domain.

The bulk temperature calculated in the bulk flow region at several values of k_{SiC} and σ_{SiC} (Fig. 12) shows that k_{SiC} has a stronger effect on the exit temperature than σ_{SiC}. The variations in the exit temperature are mostly related to heat losses from the bulk flow. The heat losses can be reduced or even fully eliminated by choosing proper k_{SiC} and σ_{SiC} from the relevant range. At k_{SiC} = 2 W/m·K, almost no leakage from the bulk flow occurs regardless of σ_{SiC}, indicating ideal thermal insulation conditions. Slightly higher bulk temperature at higher σ_{SiC} can be observed since a small amount of heat generated in the FCI is taken up by the near-wall jet.

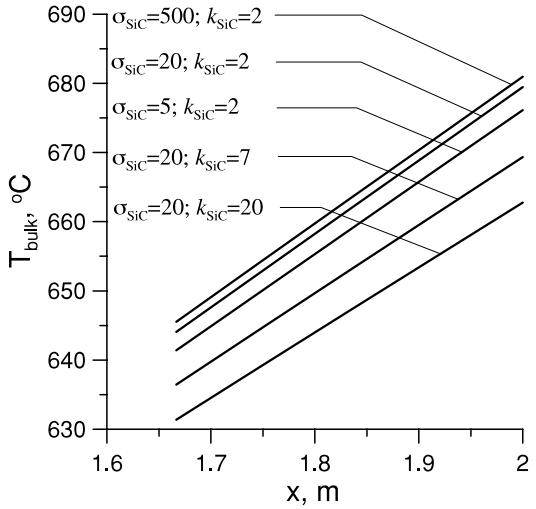

Fig. 12. Effect of k_{SiC} and σ_{SiC} on the bulk temperature.

VII. REQUIREMENTS ON k_{SiC} AND σ_{SiC}

Table II summarizes the most important flow/heat transfer parameters calculated for the case with no openings in the FCI. These data can be used to address the question of which σ_{SiC} and k_{SiC} are needed to satisfy basic design requirements imposed by the material limits and other restrictions. It is seen that the reduction of σ_{SiC} will result in lower pressure losses but in a higher temperature drop across the FCI, $(\Delta T)_{FCI}$, and in a higher interface temperature between the liquid metal and the ferritic wall, $T_{Fe\text{-}PbLi}$, at the same time. The first row of Table II, corresponding to σ_{SiC} = 5 S/m and k_{SiC} = 2 W/m·K, gives an example of intolerably high interface temperature (538°C) and fairly high temperature drop across the FCI (256°C), which will likely result in thermal stresses beyond the acceptable limit, although the

TABLE II

Summary of MHD/Heat Transfer Calculations for the Case with No Openings in the FCI

σ_{SiC} (S/m)	k_{SiC} (W/m·K)	$(\Delta T)_{FCI}$ (°C)	$T_{Fe\text{-}PbLi}$ (°C)	T_{SiC} (°C)	R	U_{jet}/U_0	$U_{Ha\ gap}/U_0$	$U_{side\ gap}/U_0$
5	2	256	538	821	190	1.41	0.00	0.49
20	2	178	526	727	62	2.30	0.01	0.99
50	2	129	517	666	28	3.44	0.03	1.79
100	2	101	512	631	15	4.64	0.05	2.82
200	2	82	508	608	8	6.10	0.09	4.51
500	2	72	504	592	4	8.23	0.20	8.23
20	7	100	552	684	62	2.30	0.01	0.99
20	20	47	570	654	62	2.30	0.01	0.99

MHD pressure drop reduction factor is high (190). As a compromise solution, we would recommend $\sigma_{SiC} \sim 100$ S/m. As for the thermal conductivity, the goal would be its minimization to $k_{SiC} \sim 2$ W/m·K since this value seems to provide low heat losses as well as acceptable $T_{Fe\text{-}PbLi}$ and low enough $(\Delta T)_{FCI}$. However, further decrease in k_{SiC} may result in $(\Delta T)_{FCI}$ to be too high. It should be noted that another blanket design or another thermal load will possibly require different values.

VIII. DISCUSSION OF 3-D EFFECTS

The present 2-D MHD analysis reflects our current understanding of MHD phenomena in the liquid metal blanket and is also limited by the available numerical tools. Although development of new high Hartmann number 3-D MHD codes[18] or modification of commercial CFD software[19,20] are in progress, the codes are not applicable yet to fusion conditions. It is therefore reasonable to discuss here what 3-D effects will likely appear and how they can affect blanket performance, leaving detailed 3-D numerical computations for the future.

The temperature differences in the flow caused by a nonuniform volumetric heating, Eq. (6), will be a cause of a 3-D convective motion driven by the buoyancy effects. An initial study for the U.S. DCLL DEMO blanket showed that the convective motion can be even stronger than the forced flow, in spite of some suppression of the convective flows by a strong 4-T magnetic field.[21] Although the effect of natural convection on the blanket performance has not been justified yet, the circulation convective motion in the bulk is expected to result in a more uniform temperature distribution, thus reducing the temperature difference on both sides of the FCI. On the other hand, heat transfer enhancement in the near-wall region owing to natural convection will provide better conditions for heat leakage from the bulk flow. Heat transfer intensification in the bulk flow will also occur due to 2-D MHD turbulence. Both mechanisms of heat transfer intensification are expected to be strong. A preliminary study of 2-D turbulence under DEMO conditions was started in Ref. 21, which showed an increase in the effective thermal conductivity in the bulk flow by a factor of 10.

A possible 3-D effect is related to temperature variations in the material properties, σ_{SiC}, first of all, due to the temperature increase in the bulk flow from 460 to 660°C as the liquid proceeds poloidally. In such a temperature range, the electric conductivity of the SiC composite can vary by a factor of 2 or even higher,[16] resulting in complex 3-D MHD effects on both the velocity and temperature field, and also causing higher MHD pressure drop. It should be mentioned that anticipated values of σ_{SiC} are in the range where small changes in σ_{SiC} can result in significant changes in the MHD pressure drop as seen in Fig. 9a. Therefore, the effect of temperature on the electric conductivity can be very important. However, qualification of such effects is a real challenge; to our best knowledge, no relevant studies under blanket conditions have been performed yet. Among other vital effects on the flows in the blanket are the multichannel effect owing to leaking currents between several poloidal ducts and spatial variations of the magnetic field. Although gradual, these variations may be important especially if the flow turns out to be turbulent.

IX. CONCLUSIONS

Basic characteristics of MHD flow and heat transfer in the front poloidal channel of the DCLL blanket with a SiC_f/SiC FCI were studied with numerical simulations using the U.S. DEMO blanket as a prototypical design. Under the particular conditions used in the analysis, parameters of the SiC_f/SiC FCI have been identified that minimize the MHD pressure drop and heat leakage from the breeder into the helium flows. Among the most important findings are the following.

1. In addition to the pressure equalization mechanism due to liquid metal flows through the openings in the FCI, an electromagnetic mechanism has been identified. With this mechanism, pressure equalization will likely occur through induced electric currents, which tend to restore the pressure balance by flowing from a higher to lower potential region through the FCI. The electromagnetic mechanism can be dominant during disruption events.

2. Between two possible locations of the PES (either in the side or Hartmann wall), the case with the PES in the Hartmann wall looks more preferable because the MHD pressure drop is lower and, unlike the case with the PES in the side wall, reverse flows do not appear.

3. The anisotropy in the electric conductivity of the insert has a small effect. The pressure drop and the velocity profile are controlled by the electrical conductivity across the fibers, while conductivity along the fibers does not play a significant role, providing that it is still much lower than the electrical conductivity of Pb-17Li.

4. The optimal combination of material properties of the SiC composite depends strongly on the thermofluid MHD and should be determined by design tradeoffs. The decrease in σ_{SiC} reduces the MHD pressure drop but at the same time leads to a higher temperature drop across the FCI (higher thermal stress) and higher interface temperature between the ferritic wall and the Pb-17Li. The following values of electric and thermal conductivity can be recommended to meet basic design requirements: $\sigma_{SiC} \sim 100$ S/m; $k_{SiC} \sim 2$ W/m·K.

5. Performance of the blanket will be affected by such phenomena as buoyancy effects, 2-D MHD turbulence, and temperature changes of σ_{SiC}.

ACKNOWLEDGMENTS

The study has been performed under U.S. Department of Energy grant DE-FG02-86ER52123-A040. We would like to acknowledge the contribution of many people: M. Sawan for the neutronics calculations; S. Malang and C. Wong for their numerous comments in the course of the study; R. Moreau for the cooperation on buoyancy effects and 2-D MHD turbulence; S. Zinkle, J. Youngblood, and Y. Katoh for the information on SiC_f/SiC properties; and S. Molokov for reading the manuscript and his help with the references.

REFERENCES

1. M. S. TILLACK and S. MALANG, "High Performance PbLi Blanket," *Proc. 17th IEEE/NPSS Symp. Fusion Engineering*, San Diego, California, October 6–10, 1997, Vol. 2, p. 1000, Institute of Electrical and Electronics Engineers/Nuclear and Plasma Sciences Society (1997).

2. ARIES TEAM, M. S. TILLACK, X. R. WANG, J. PULSIFER, S. MALANG, and D. K. SZE, "ARIES-ST Breeding Blanket Design and Analysis," *Fusion Eng. Des*., **49–50**, 689 (2000).

3. P. NORAJITRA et al., "The EU Advanced Lead Lithium Blanket Concept Using SiC_f/SiC Flow Channel Inserts as Electrical and Thermal Insulators," *Fusion Eng. Des*., **58–59**, 629 (2001).

4. C. WONG et al., "Assessment of Liquid Breeder First Wall and Blanket Options for the DEMO Design," *Fusion Sci. Technol*., **47**, 502 (2005).

5. M. ABDOU et al., "US Plans and Strategy for ITER Blanket Testing," *Fusion Sci. Technol*., **47**, 475 (2005).

6. P. NORAJITRA et al., "Conceptual Design of the Dual-Coolant Blanket Within the Framework of the EU Power Plant Conceptual Study (TW2-TPR-PPCS12). Final Report," FZKA 6780, Forschungszentrum Karlsruhe (May 2003).

7. S. SMOLENTSEV et al., "Numerical Analysis of MHD Flow and Heat Transfer in a Poloidal Channel of the DCLL Blanket with a SiC_f/SiC Flow Channel Insert," *Fusion Eng. Des.*, **81**, 549 (Feb. 2006).

8. S. MOLOKOV and A. SHISHKO, "Fully Developed Magnetohydrodynamic Flows in Rectangular Ducts with Insulating Walls," KfK 5247, Kernforschungszentrum Karlsruhe (1993).

9. J. H. DAVIDSON and F. A. KULACKI, "Convective Heat Transfer with Electric and Magnetic Fields," *Handbook of Single-Phase Convective Heat Transfer*, S. KAKAC, R. K. SHAH, and W. AUNG, Eds., John Wiley & Sons (1987).

10. R. MOREAU, *Magnetohydrodynamics*, Kluwer (1990).

11. S. SMOLENTSEV, N. B. MORLEY, and M. ABDOU, "Code Development for Analysis of MHD Pressure Drop Reduction in a Liquid Metal Blanket Using Insulation Technique Based on a Fully Developed Flow Model," *Fusion Eng. Des*., **73**, 83 (2005).

12. R. E. ALCOUFFE et al., "DANTSYS 3.0, A Diffusion Accelerated Neutral Particle Transport Code System," LA-12969-M, Los Alamos National Laboratory (June 1995).

13. A. R. RAFFRAY et al., "Design and Material Issues for High Performance SiC_f/SiC-Based Fusion Power Cores," *Fusion Eng. Des*., **55**, 55 (2001).

14. R. SCHOLZ, F. DOS SANTOS MARQUES, and B. RICCARDI, "Electrical Conductivity of Silicon Carbide Composites and Fibers," *J. Nucl. Mater*., **307–311**, 1098 (2002).

15. Y. KATOH et al., "Property Tailorability for Advanced CVI Silicon Carbide Composites for Fusion," *Fusion Eng. Des.*, **81**, 937 (Feb. 2006).

16. G. YOUNGBLOOD, Personal Communication (May 2005).

17. L. BÜHLER and S. MOLOKOV, "Magnetohydrodynamic Flows in Ducts with Insulating Coatings," KfK 5103, Forschungszentrum Karlsruhe (1993).

18. R. MUNIPALLI et al., "Development of a 3-D Incompressible Free Surface MHD Computational Environment for Arbitrary Geometries: HIMAG," DOE SBIR Phase-II Final Report, U.S. Department of Energy (June 2003).

19. S. ALEKSANDROVA, S. MOLOKOV, and C. B. REED, "Modeling of Liquid Metal Duct and Free-Surface Flows Using CFX," ANL/TD/TM02-30, Argonne National Laboratory (June 2002).

20. C. MISTRANGELO and L. BÜHLER, "Three-Dimensional Magnetohydrodynamic Flows in Sudden Expansions," *Proc. Joint 15th Riga and 6th Pamir Int. Conf. Fundamental and Applied Magnetohydrodynamiic*, Riga, Latvia, June 27–July 1, 2005, p. 223.

21. S. SMOLENTSEV, N. B. MORLEY, M. ABDOU, and R. MOREAU, "Current Approaches to Modeling MHD Flows in the Dual Coolant Lithium-Lead Blanket," *Proc. Joint 15th Riga and 6th Pamir Int. Conf. Fundamental and Applied Magnetohydrodynamics*, Riga, Latvia, June 27–July 1, 2005, p. 239.